Dihydroorotate Dehydrogenase from *Clostridium oroticum* Is a Class 1B Enzyme and Utilizes a Concerted Mechansim of Catalysis†

Argyrides Argyrou,‡,§ Michael W. Washabaugh,‖ and Cecile M. Pickart*,‡

Department of Biochemistry and Molecular Biology, The Johns Hopkins University, Baltimore, Maryland 21205, and Merck & Company, Inc., P.O. Box 4, West Point, Pennsylvania 19486

Received May 16, 2000

ABSTRACT: Dihydroorotate dehydrogenase from *Clostridium oroticum* was purified to apparent homogeneity and found to be a heterotetramer consisting of two α (32 kDa) and two β (28 kDa) polypeptides. This subunit composition, coupled with known cofactor requirements and the ability to transfer electrons from L-dihydroorotate to NAD^+, defines the *C. oroticum* enzyme as a family 1B dihydroorotate dehydrogenase. The results of steady-state kinetic analyses and isotope exchange studies suggest that this enzyme utilizes a ping-pong steady-state kinetic mechanism. The pH−k_{cat} profile is bell-shaped with a pK_a of 6.4 ± 0.1 for the ascending limb and 8.9 ± 0.1 for the descending limb; the pH−k_{cat}/K_m profile is similar but somewhat more complex. The pK_a values of 6.4 and 8.9 are likely to represent the ionizations of cysteine and lysine residues in the active site which act as a general base and an electrostatic catalyst, respectively. At saturating levels of NAD^+, the isotope effects on ^DV and $^D(V/K_{DHO})$, obtained upon deuteration at both the C_5-*proR* and C_5-*proS* positions of L-dihydroorotate, increase from a value of unity at pH >9.0 to sizable values at low pH due to a high commitment to catalysis at high pH. At pH = 6.5, the magnitude of the double isotope effects ^DV and $^D(V/K_{DHO})$, obtained upon additional deuteration at C_6, is consistent with a mechanism in which C_5-*proS* proton transfer and C_6-hydride transfer occur in a single, partially rate-limiting step.

Dihydroorotate dehydrogenase (DHO dehydrogenase;[1] EC 1.3.1.14, EC 1.3.3.1, EC 1.3.99.11) catalyzes the conversion of L-DHO (**1**, Scheme 1) to orotate (**3**, Scheme 1). This conversion is the fourth step, and the sole redox reaction, in the pyrimidine biosynthetic pathway. The reaction proceeds with stereospecific abstraction of the C_5-*proS* proton of L-DHO (*1*, *2*), followed by (or concomitant with) C_6-hydride delivery to a tightly bound flavin, resulting in the *trans*-dehydrogenation of the substrate. The electron acceptor used to reoxidize the enzyme varies with the enzyme source. We have studied the *Clostridium oroticum* (originally named *Zymobacterium oroticum*) enzyme which employs NAD^+ (*3*) as the ultimate electron acceptor (eq 1).

$$\text{L-DHO} + \text{NAD}^+ \underset{\text{DHase}}{\overset{\text{DHO}}{\rightleftharpoons}} \text{OA} + \text{NADH} + \text{H}^+ \qquad (1)$$

Scheme 1

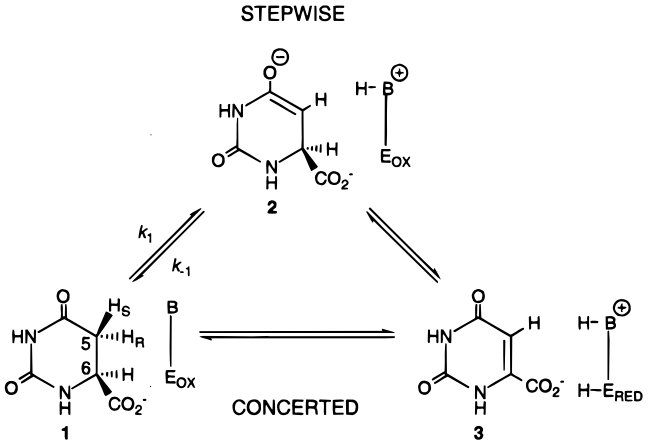

Sequence analyses have defined two families of DHO dehydrogenases (*4*). Family 2 consists of membrane-bound enzymes, including those of *Escherichia coli* and the mitochondria of higher eukaryotes. These enzymes use a quinone as the ultimate electron acceptor. Family 1 enzymes are soluble and cytosolic; they can be further divided into two subfamilies. Subfamily 1A includes one of the two enzymes from *Lactococcus lactis* as well as the enzymes from *Saccharomyces cerevisiae* and *Trypanosoma cruzi* (*5*). The *L. lactis* A enzyme, a homodimer with one molecule of FMN per subunit, uses fumarate as the ultimate electron

† Supported by NIH Grant DK46984. A.A. is a recipient of the Elsa Orent Keiles fellowship for nutritional research.

* Corresponding author: tel, (410) 614-4554; fax, (410) 955-2926; e-mail, cpickart@welchlink.welch.jhu.edu.

‡ The Johns Hopkins University.

§ Present address: Department of Biochemistry, Albert Einstein College of Medicine, 1300 Morris Park Ave., Bronx, NY 10461.

‖ Merck and Co., Inc.

[1] Abbreviations: bis-tris, 2,2-bis(hydroxymethyl)-2,2′,2″-nitrilotriethanol; bis-tris propane, 1,3-bis[[tris(hydroxymethyl)methyl]amino]-propane; L-DHO, L-dihydroorotate; DHO dehydrogenase, dihydroorotate dehydrogenase; Me_2SO-d_6, deuterated dimethyl sulfoxide; D_2O, deuterium oxide; FMN, flavin mononucleotide; FAD, flavin adenine dinucleotide; NAD^+, β-nicotinamide adenine dinucleotide; OA, orotate; SDS−PAGE, sodium dodecyl sulfate−polyacrylamide gel electrophoresis; TLC, thin-layer chromatography; tris, tris(hydroxymethyl)-aminomethane.

10.1021/bi001111d CCC: $19.00
Published on Web 08/04/2000

acceptor (*6*). Subfamily 1B consists of the enzymes from Gram-positive bacteria, including the *L. lactis* B enzyme (*7*), the *Bacillus subtilis* enzyme (*8*), and the *Enterococcus faecalis* enzyme (*9*). These prototypical class 1B enzymes are $\alpha_2\beta_2$ heterotetramers and utilize a remarkable array of prosthetic groups: there are two molecules of FMN, two molecules of FAD, four non-heme iron atoms, and four labile sulfur atoms per heterotetramer. Family 1B enzymes use NAD^+ as the ultimate electron acceptor.

A question of fundamental importance in enzymology is how enzymes handle moderately unstable carbanions such as the C_5-carbanion/enolate of L-DHO (**2**, Scheme 1). Scheme 1 shows two mechanisms by which DHO dehydrogenase could catalyze the oxidation of L-DHO: (i) a stepwise mechanism involving a C_5-carbanion/enolate intermediate (upper pathway) or (ii) a concerted mechanism that avoids this intermediate (lower pathway). Which pathway is utilized depends in part on the thermodynamic stability (pK_a) of the carbon acid (*10*, *11*). We recently estimated a $pK_a \approx 20-21$ for the C_5-*proS* proton of L-DHO in solution (*12*), whereas a $pK_a \leq 18.3$ is required for the C_5-carbanion/enolate to be an intermediate in a stepwise mechanism of catalysis by DHO dehydrogenase (*10*, *12*). Thus, the enzyme either stabilizes the C_5-carbanion/enolate relative to **1** (or raises the pK_a of an enzymatic general base by ≥ 1.7 pK_a units) or avoids the formation of the unstable carbanion by providing a one-step, concerted pathway. Comparison of the non-enzymatic second-order rate constant for catalysis of C_5-*proS* proton exchange by a buffer of $pK_a = 7.2$ (*12*) with the catalytic efficiency of DHO dehydrogenase [$k_{cat}/K_{m(DHO)}$] allowed us to estimate a rate enhancement of $\approx 10^{10}$ for enzyme-catalyzed C_5-*proS* proton abstraction if the mechanism is stepwise.

To distinguish between stepwise and concerted mechanisms for the enzyme-catalyzed reaction, we purified DHO dehydrogenase from *C. oroticum* and used multiple isotope effects to probe its mechanism. The results are fully consistent with a concerted mechanism of catalysis and are inconsistent with a stepwise mechanism. The properties of DHO dehydrogenase from *C. oroticum* indicate that this enzyme belongs to family 1B. A comparison of the present results with those obtained in earlier studies of the enzymes from *Crithidia fasciculata* (family 1A) (*2*) and bovine liver mitochondria (family 2) (*13*) suggests that the distinct structural properties of the three enzyme families may be paralleled by distinct catalytic mechanisms.

EXPERIMENTAL PROCEDURES

Materials. All chemicals were of analytical or reagent grade and were used without further purification unless otherwise stated. [6-^{14}C]Orotic acid (40 μCi/μmol) was from ICN. L-DHO (Sigma) was recrystallized from water: mp = 265−269 °C dec (lit. 266 °C) (*14*). Orotic acid, NAD^+, NADH, and pyruvate were from Sigma. D_2O (99.9 atom % D), methanol-*d* (99.5+ atom % D), sodium methoxide, and deuterated dimethyl sulfoxide (Me_2SO-d_6) were from Aldrich. *C. oroticum* was obtained from the American Type Culture Collection. Water was prepared on a four-bowl Milli-Q water system including an Organex-Q cartridge (Millipore).

General Methods. Protein concentrations were determined with bicinchoninic acid (*15*) using bovine serum albumin as standard. The solution pH was measured at 25 °C with an Orion Model SA 720 pH meter and Radiometer GK2321C combination electrode standardized at pH 7.00 and 4.00 or 10.00. Melting points were determined using an electrothermal digital melting point apparatus and are uncorrected. ^{1}H NMR spectra were recorded on a Bruker AMX-300 NMR spectrometer. For samples in Me_2SO-d_6, the residual methyl protons of Me_2SO were used as an internal chemical shift standard ($\delta = 2.49$ ppm). For samples in D_2O, 3-(trimethylsilyl)propanesulfonate was used as an internal chemical shift standard.

Growth of Bacteria. C. oroticum was grown at pH 7.5 in a medium described previously (*16*), which included orotic acid (4 g/L) to induce the expression of DHO dehydrogenase. Medium (500 mL) was inoculated with 2.5 mL of actively growing culture (freshly prepared medium was used to avoid precipitation of orotic acid, which otherwise occurred after 12 h at room temperature). Flasks were maintained anaerobically (90% N_2, 5% CO_2, 5% H_2) at 35−37 °C without shaking, and bacteria were harvested after ≤15 h of growth. Typically, 2.5 g of cells (wet weight) was obtained per liter of culture.

Purification of DHO Dehydrogenase. All operations were carried out on ice or at 4 °C. Cell paste (10 g) was suspended in 40 mL of 50 mM tris-HCl, pH = 6.8, 5 mM L-cysteine, and 10 mM orotate, and the suspension was incubated in vacuo (*3*) at 25 °C for 30 min. Leupeptin (1 μg/mL), phenylmethanesulfonyl fluoride (0.1 mM), and lysozyme (1 mg/mL) were then added, and the cells were disrupted by sonication. Cell debris was removed by centrifugation at 20000*g* for 90 min, and proteins precipitating from the supernatant between 50% and 65% saturation with $(NH_4)_2SO_4$ (*16*) were collected. The pellet was dissolved in 4 mL of 50 mM sodium phosphate buffer, pH = 6.5, dialyzed for 4 h against 2 L of 50 mM sodium phosphate buffer, pH = 6.5, and clarified by centrifugation. The dialysate was applied to a 20 mL column of Q-Sepharose FF (Amersham-Pharmacia Biotech) equilibrated with 20 mM bis-tris, pH = 6.5. The column was washed with 60 mL of the same buffer and then eluted with a linear gradient (400 mL) from 0 to 0.6 M NaCl in 20 mM bis-tris, pH = 6.5; fractions of 5 mL were collected. The orange-brown fractions containing DHO dehydrogenase, which eluted at ≈0.27 M NaCl, were pooled (30 mL) and applied directly to a 6.5 mL Bio-Gel HTP hydroxyapatite column (Bio-Rad) equilibrated with 0.3 M sodium phosphate, pH = 5.8. The column was washed with 56 mL of the same buffer, followed by elution with 56 mL of 0.27 M sodium phosphate, pH = 6.3. Fractions of 2.5 mL were collected. The active fractions were pooled and stored in small aliquots at −20 °C. The specific activity of the purified protein, at saturating concentrations of L-DHO and NAD^+, was 2600 mol of orotate formed min^{-1} (mol of enzyme tetramer)$^{-1}$ using assay 2 (below). Loss of activity was <15% over 6 months. Analytical gel filtration of the enzyme (Results) was carried out on a calibrated Sephacryl-200 column (Amersham-Pharmacia Biotech).

Enzymes. The same preparation of purified *C. oroticum* DHO dehydrogenase ($A_{272}/A_{454} = 4.0$) was used for all kinetic experiments. The enzyme concentration was determined from $\epsilon_{454} = 67.3$ mM^{-1} (tetramer) cm^{-1} (*16*). For the enzymatic synthesis of compounds **1** and **4**−**6** (see below), commercial *C. oroticum* DHO dehydrogenase (Sigma) was used without

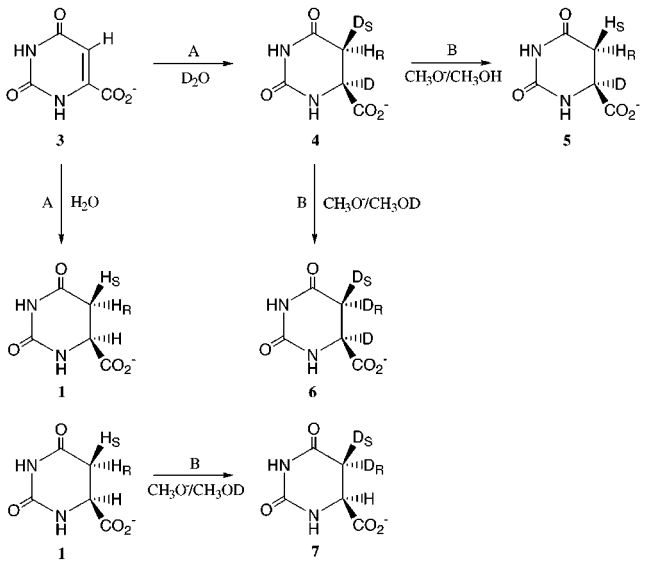

FIGURE 1: Synthesis of L-DHO molecules selectively labeled with deuterium. A denotes enzymatic synthesis using *C. oroticum* DHO dehydrogenase. B denotes chemical exchange of the C_5-hydrons of L-DHO using sodium methoxide in methanol or methanol-*d*.

further purification. Rabbit muscle L-lactate dehydrogenase from Sigma (no. L 1254) was used without further purification.

Synthesis of Deuterated L-DHO Molecules (Figure 1). Procedures were modified from those published previously (*2*).

(A) L-*[5S,6-$^2H_2$]-DHO (**4**).* Sodium phosphate (0.2 M), pD = 6.6, 1 mM EDTA, 10 mM L-cysteine, 5 mM sodium orotate, and 3.75 units of *C. oroticum* DHO dehydrogenase in a 25 mL reaction in D_2O were incubated at 25 °C. After 10 min, NADH (10 mM) was added and the solution incubated for 11 h at 25 °C. The reaction mixture was applied directly to a column of Dowex 1X8−400 (Sigma, 20 mL bed volume) and eluted with 70 mM sodium formate adjusted to pH = 3.2 with formic acid. [The column had been previously treated successively with (a) 100 mL of 1 N NaOH/1 M NaCl, (b) 100 mL of water, (c) 100 mL of 1 N HCl, (d) 100 mL of water, and (e) 200 mL of 70 mM sodium formate adjusted to pH = 3.2 with formic acid.] Fractions 12−25 (8 mL per fraction) were pooled and passed through a column of Dowex 50WX8−400 (Sigma, 20 mL bed volume) and eluted with water to remove the sodium ions. [The column had been previously treated successively with (a) 100 mL of 1 N NaOH/1 M NaCl, (b) 100 mL of water, (c) 100 mL of 1 N HCl, and (d) 200 mL of water.] Fractions 2−17 (8 mL per fraction) were pooled, and the solvent was evaporated. The residue was crystallized from water to yield compound **4** (35% yield, 6 mg): mp 265−268 °C dec; ^{1}H NMR (Me_2SO-d_6) δ 13.11 (s, 1H, $-CO_2-$**H**), 10.09 (s, 1H, $-N_3-$**H**), 7.75 (s, 1H, $-N_1-$**H**), 2.86 (s, 1H, $-C_5$-*proR*−**H**). The NMR spectrum indicated that the C_5-*proS*−H and C_6−H were >96% deuterated.

(B) L-*DHO (**1**).* This control molecule was synthesized to be compared with that obtained from Sigma (see Results). Orotate was reduced by *C. oroticum* DHO dehydrogenase as described for compound **4**, except that the solvent was H_2O instead of D_2O. Purification and crystallization as described above yielded **1** (32% yield, 5.5 mg): mp 265−268 °C dec; ^{1}H NMR (Me_2SO-d_6) δ 13.10 (s, 1H, $-CO_2-$**H**), 10.08 (s, 1H, $-N_3-$**H**), 7.75 (s, 1H, $-N_1-$**H**), 4.06 (p, 1H, $-C_6-$**H**), 2.87 (q, 1H, $-C_5$-*proR*−**H**), 2.54 (q, 1H, $-C_5$-*proS*−**H**).

(C) L-*[6-^{2}H]-DHO (**5**).* The first step for the synthesis of this molecule was the same as that for **4** except that the crystallization step was omitted. The residue obtained after evaporation of solvent was dissolved in 25 mL of methanol containing 0.235 g of sodium methoxide (0.17 M). The solution was sonicated for 3 h in a water bath sonicator. The solvent was evaporated and the residue resuspended in 25 mL of 0.17 M HCl and loaded directly on a Dowex 50WX8−400 column (pretreated as described above) to remove the sodium ions. Fractions 2−9 (8 mL per fraction) were pooled, the solvent was evaporated, and the residue was crystallized from water to yield compound **5** (35% yield, 6 mg): mp 265−268 °C dec; ^{1}H NMR (Me_2SO-d_6) δ 13.10 (s, 1H, $-CO_2-$**H**), 10.08 (s, 1H, $-N_3-$**H**), 7.74 (s, 1H, $-N_1-$**H**), 2.87 (d, 1H, $-C_5$-*proR*−**H**), 2.54 (d, 1H, $-C_5$-*proS*−**H**). The NMR spectrum indicated that the C_6−H was >96% deuterated.

(D) L-*[5R,5S,6-$^2H_3$]-DHO (**6**).* The synthesis of **6** was essentially the same as that for **5**, except that methanol-*d* replaced methanol. Isolation and crystallization as before yielded **6** (32% yield, 5.5 mg): mp 265−268 °C dec; ^{1}H NMR (Me_2SO-d_6) δ 13.03 (s, 1H, $-CO_2-$**H**), 10.08 (s, 1H, $-N_3-$**H**), 7.74 (s, 1H, $-N_1-$**H**). On the basis of the NMR spectrum, deuterium was enriched at each position as indicated: C_5-*proR*−H (>96%), C_5-*proS*−H (>96%), and C_6−H (>97%).

(E) L-*[5R,5S-$^2H_2$]-DHO (**7**).* L-DHO (0.2 g) (Sigma) was dissolved in 50 mL of methanol-*d* containing 0.47 g of sodium methoxide (0.17 M) and sonicated for 3 h in a water bath sonicator. After evaporation of solvent, the residue was dissolved in 25 mL of 0.34 M HCl and loaded directly onto Dowex 50WX8−400 and purified as described above. Isolation and crystallization yielded **7** (0.12 g, 60% yield): mp 265−268 °C dec; ^{1}H NMR (Me_2SO-d_6) δ 13.09 (s, 1H, $-CO_2-$**H**), 10.08 (s, 1H, $-N_3-$**H**), 7.75 (d, 1H, $-N_1-$**H**), 4.04 (d, 1H, $-C_6-$**H**). The NMR spectrum indicated that the C_5-*proR*−H and C_5-*proS*−H were >97% deuterated.

The 300 MHz ^{1}H NMR spectra of samples of deuterated and nondeuterated L-DHO showed no significant peaks other than those expected from L-DHO and NMR solvents (not shown).

Determination of Substrate Concentrations. Stock solutions of deuterated and nondeuterated L-DHO were prepared in water, and NaOH was added to give 90% deprotonation of the C_6-carboxylic acid (pH ≈3.5). The concentration of L-DHO in stock solutions was determined by completely oxidizing an aliquot using purified *C. oroticum* DHO dehydrogenase. Reactions contained 50 mM bis-tris propane/50 mM phosphate, pH = 8.0, 10 mM L-cysteine, 1 mM EDTA, 2 mM pyruvate, 0.02 unit/μL rabbit muscle L-lactate dehydrogenase, 40−70 nM enzyme, and 0.2 mM NAD^+. After preincubation for 20 min, the reaction was initiated by adding L-DHO to 0.1 mM. The increase in absorbance at 295 nm due to the formation of orotate ($\epsilon_{pH\ 8.0}$ = 4.23 mM^{-1} cm^{-1}) permitted the determination of the original L-DHO concentration to within ≤±3%. Gravimetrically prepared solutions of L-DHO verified the precision of this method.

Enzyme Assays. Assays were done at 25 °C. Initial rates were determined from linear plots of product formation (or

substrate disappearance) under conditions of ≤8% substrate conversion.

Assay 1. Assay 1, used during purification, monitored the reduction of orotate (reverse of eq 1 above). Enzyme was preincubated for 10 min in 50 mM MES buffer, pH = 6.5, 10 mM L-cysteine, and 2.5 mM orotate, and the reaction was initiated by addition of NADH to 0.17 mM. Conversion of NADH to NAD^+ was monitored at 340 nm.

Assay 2. Assay 2 monitored oxidation of L-DHO through the increase in absorbance at 290−300 nm due to production of orotate (the extinction coefficients for orotate at 290, 295, and 300 nm at 5.0 ≤ pH ≤ 8.5 and 25 °C were 5.96, 4.23, and 2.69 mM^{-1} cm^{-1}, respectively; the extinction coefficients for orotate at 300 nm were 2.92, 3.52, and 3.69 mM^{-1} cm^{-1} at pH 9.0, 9.5, and 10.0, respectively). An NAD^+-regenerating system (L-lactate dehydrogenase converts NADH to NAD^+ during reduction of pyruvate to L-lactate) was included to make this thermodynamically unfavorable reaction irreversible (see Results). (Note that NAD^+ also absorbs at 290−300 nm, but its concentration does not change during the assay.) Assays contained 50 mM acetate/50 mM phosphate (5.0 ≤ pH ≤ 7.0) or 50 mM bis-tris propane/50 mM phosphate (6.0 ≤ pH ≤ 10.0), 10 mM L-cysteine, 1 mM EDTA, 2 mM pyruvate, 0.02 unit/μL rabbit muscle L-lactate dehydrogenase, DHO dehydrogenase, and NAD^+. All components except L-DHO were preincubated at 25 °C for 20 min, and reactions were initiated by addition of L-DHO.

Assay 3: Anaerobic Isotope Exchange Experiments. Anaerobic conditions were attained by repeated (10 times) evacuation and flushing with nitrogen of a disposable glovebag. Nitrogen was then bubbled through all buffers and solutions (except enzyme) for 20 min inside the glovebag. Assays (50 μL) contained 50 mM bis-tris propane/50 mM phosphate, pH = 8.0, 10 mM L-cysteine, 1 mM EDTA, 1 mM [6-^{14}C]orotate (0.01 μCi/μL), L-DHO (0.5−4 mM), and 100 nM (tetramer) DHO dehydrogenase. After a 20 min preincubation, the reaction was initiated by addition of L-DHO. Aliquots of 0.5 μL were removed at timed intervals and spotted onto polyethylenimine−cellulose-F TLC plates (EM Science) in which the origins had been pretreated with 1 μL of 0.46 N formic acid and air-dried. The TLC plates were developed with 0.46 N formic acid, air-dried, and exposed to a phosphorimaging plate (Fuji) for 1 h. This chromatographic system afforded excellent separation of orotate (R_f = 0.1) from L-DHO (R_f = 0.5). Initial rates of radiolabeled L-DHO formation were calculated from the linear slopes of plots of [L-DHO] against time.

Controls for pH−Rate Studies. To be certain that the pH dependence of kinetic parameters (see Results) was not due to a lower amount of active enzyme such as would result from the lower concentration of activating thiolate anion at low pH, L-cysteine (pK_a = 8.3) and D-cysteine were titrated at pH = 5.0 and pH = 8.0. The total concentration of L-cysteine or D-cysteine required for half-maximal activation ($S_{0.5}$) was 2.5 mM at pH = 5.0 and 1.8 mM at pH = 8.0. Since the $S_{0.5}$ values for L-cysteine are similar at pH = 5.0 and pH = 8.0, and since all kinetic experiments were done at 10 mM L-cysteine, the pH dependence of the kinetic parameters cannot be attributed to the ionization state of the activating thiol. Doubling or halving the concentration of L-lactate dehydrogenase or pyruvate had no effect on the observed velocities at pH = 5.0, 8.0, or 10.0 with the highest concentrations of substrates used, indicating that regeneration of NAD^+ was not limiting at any pH. The concentration of NAD^+ was 2 mM in all of the assays. This concentration is saturating at pH 8.0 [∼15 × K_m; true $K_{m(NAD^+)}$ at pH 8.0 = 130 μM]. Although the $K_{m(NAD^+)}$ may be different at low or high pH, halving the concentration of NAD^+ (from 2 mM to 1 mM) at pH = 5.0, 8.0, and 10.0 gave only a 7−10% decrease in the observed velocities. Thus, NAD^+ was close to saturation across the entire pH profile.

N-Terminal Sequence Analysis. Purified *C. oroticum* DHO dehydrogenase (∼3 μg) was resolved by SDS−PAGE. The two subunits (see Results) were electrophoretically transferred to a PVDF membrane (Millipore). The subunits were located on the blot by staining with Ponceau S, excised, and subjected to N-terminal sequence analysis in the facility of the Biological Chemistry Department in The Johns Hopkins University School of Medicine. Although the N-terminal sequences for the α (SRLKTEFAGA) and β (GKILTNVRLS) subunits were not detectably similar to those of the family 1B enzymes, we note that the extreme N-termini of this enzyme family are not well conserved.

Data Analysis. All fits were done using the Sigmaplot (version 4.16) linear or nonlinear least-squares curve-fitting program for the Macintosh.

Reciprocal initial velocities (1/*V*) were plotted against reciprocal substrate concentrations (1/*S*), and the data were fitted to eq 2. The slope is K_m^{app}/V_{max}^{app}, and the *Y*-intercept is $1/V_{max}^{app}$.

$$1/V = K_m^{app}/(V_{max}^{app}S) + 1/V_{max}^{app} \quad (2)$$

Data for pH−rate profiles were fitted to eq 3 or 4. Data showing a decrease in log *V* or log *V*/*K* at low and high pH were fitted to eq 3. When log *V* or log *V*/*K* decreased at both low and high pH but showed a hollow at low pH, the data were fitted to eq 4. In these equations, *y* is *V* or *V*/*K*, *C* is the pH-independent value of *V* or *V*/*K*, *H* is [H^+], and K_A−K_D represent the dissociation constants for groups on the enzyme and/or substrates.

$$\log y = \log [C/(1 + H/K_B + K_D/H)] \quad (3)$$

$$\log y = \log \{C[1 + H/K_A]/[1 + (H/K_B)(1 + H/K_C) + K_D/H]\} \quad (4)$$

For the pH dependence of the primary deuterium kinetic isotope effect, the data were fitted to eq 5, where IE_{obsd} is the observed isotope effect at a particular pH, IE_{LpH} is the pH-independent isotope effect at low pH, and pK_a is the pH at which the observed isotope effect is half the value of IE_{LpH}.

$$IE_{obsd} = IE_{LpH}/(1 + 10^{pH-pK_a}) + 1/(1 + 10^{pK_a-pH}) \quad (5)$$

RESULTS

C. oroticum DHO Dehydrogenase Is a Family 1B Enzyme. To obtain large quantities of DHO dehydrogenase for mechanistic studies, we took advantage of the induction of enzyme expression that occurs when *C. oroticum* is cultured in the presence of orotic acid (*17*). We developed a simple purification procedure (Experimental Procedures) that gave a high yield of enzyme: ∼2.8 mg of enzyme was obtained in 13% yield from 4 L of cultured cells. A 52-fold increase

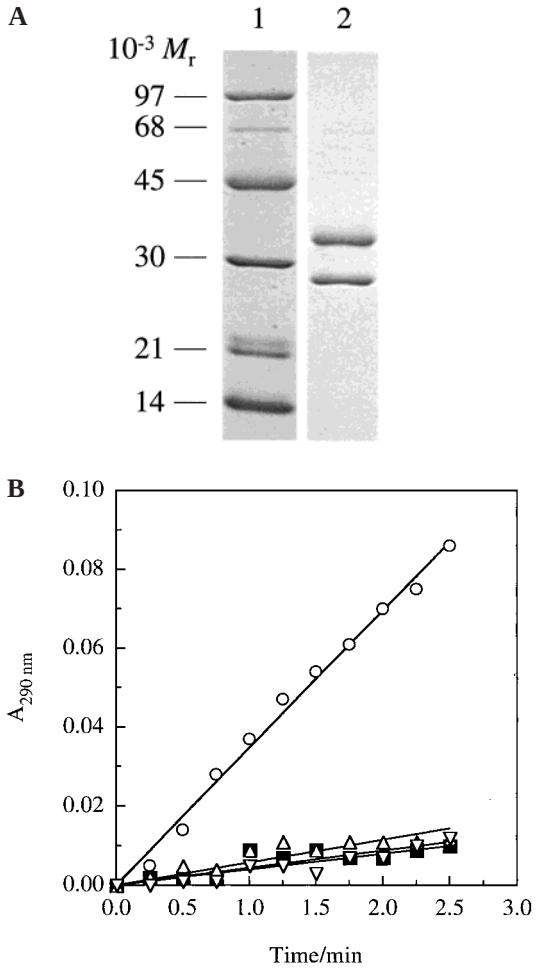

FIGURE 2: (A) SDS−polyacrylamide gel electrophoretic analysis of purified *C. oroticum* DHO dehydrogenase. Lane 1 contains protein molecular weight markers; lane 2 contains 6 μg of purified *C. oroticum* DHO dehydrogenase. (B) Typical time courses for *C. oroticum* DHO dehydrogenase showing activation of the enzyme by 10 mM L-cysteine (○) relative to unactivated enzyme (■) but not by L-alanine (△) or L-serine (▽). *C. oroticum* DHO dehydrogenase (4.7 nM) was preincubated for 20 min in the presence (or absence) of 10 mM L-cysteine, 1 mM EDTA, 0.4 mM NAD^+, 0.02 unit/μL L-lactate dehydrogenase, and 2 mM pyruvate in buffer containing 50 mM phosphate/50 mM bis-tris propane, pH = 8.0, and the reaction was initiated by addition of 1 mM L-DHO.

in specific activity was sufficient to achieve near homogeneity, indicating that the enzyme represented ~2% of total protein in the crude cell extract.

An SDS−PAGE analysis of the purified enzyme is shown in Figure 2A. There are approximately equal amounts of two polypeptides with masses of ~32 and ~28 kDa, which together constitute >90% of the Coomassie-stained protein. These two proteins were designated as the α and β subunits of a heterotetrameric DHO dehydrogenase on the basis of the following criteria. (1) The two polypeptides precisely coeluted in each purification step with respect to (a) one another, (b) NADH-dependent orotate reductase activity, and (c) yellow color (Experimental Procedures). The coelution of the two polypeptides indicates that they are the subunits of an oligomeric enzyme. (2) The results of analytical size exclusion chromatography (Experimental Procedures) showed that the two polypeptides eluted at the same position as ubiquitin activating enzyme, a protein with a native molecular mass of 116 kDa (*18*). The molecular mass of the active enzyme is thus consistent with an $\alpha_2\beta_2$ heterotetrameric structure, as seen previously for the *L. lactis* B enzyme (*7*) and the enzymes from *B. subtilis* (*8*) and *E. faecalis* (*9*). (3) Highly purified DHO dehydrogenase from *C. oroticum* was previously shown (*16*) to exhibit the cofactor content that is now recognized as typical of family 1B enzymes, namely, two molecules of FMN, two molecules of FAD, four nonheme iron atoms, and four labile sulfur atoms per mole of enzyme. This cofactor composition, in conjunction with the subunit composition demonstrated by our results, indicates that the *C. oroticum* enzyme belongs to DHO dehydrogenase family 1B.

Continuous Assay of Orotate Formation Catalyzed by DHO Dehydrogenase. The equilibrium of the reaction shown in eq 1 greatly favors reactants (*19*), making it difficult to measure initial velocities by following the production of NADH. As described in Experimental Procedures (Assay 2), we developed a new assay method in which this problem was overcome by including an NAD^+-regenerating system to make the oxidation of L-DHO irreversible. Initial velocities were then conveniently measured by following the increase in absorbance at 290−300 nm associated with orotate formation. A typical assay time course is shown in Figure 2B. Orotate was formed linearly with time (circles) at a rate that depended linearly on enzyme concentration (data not shown). As reported previously (*16*, *20*), L-cysteine activated the enzyme strongly (circles versus squares), whereas L-serine and L-alanine did not (upright and inverted triangles). Besides L-cysteine, other thiols were also activators, including D-cysteine, 2-mercaptoethanol, dithiothreitol, mercaptoacetic acid, and glutathione (*16*, *20*; data not shown). The concentration of L-cysteine required for half-maximal activity at pH = 8.0 was 1.8 mM (Experimental Procedures). A concentration of L-cysteine affording near-maximal activity, 10 mM, was used in the experiments reported below.

The mechanism by which thiols activate DHO dehydrogenase has not been definitively demonstrated. However, earlier work (*16*, *20*) showed that the NAD^+-dependent DHO dehydrogenase and NAD^+-independent DHO oxidase activities are activated by thiols, while the orotate-independent NADH oxidase activity is not. These findings suggest that thiols affect the L-DHO/orotate reaction rather than the NAD^+/NADH reaction. The crystal structure of *L. lactis* DHO dehydrogenase A without bound orotate (*4*) shows extra electron density around the sulfur atom of a crucial (*21*) active site cysteine residue (Cys-130), indicating that the cysteine sulfur was oxidized, perhaps to a sulfenic acid (−SOH). Cys-130 is conserved in family 1B enzymes (*4*). Thus, we propose that the observed thiol activation (Figure 2B) involves the reduction of the side chain of a cysteine residue corresponding to Cys-130, which would be necessary for its proposed function as a general base (see Discussion). Sulfenic acids can be reduced to thiols by thiols in solution (*22*). In contrast, there is no evidence to support an alternative mechanism in which activation involves the reduction of an inhibitory protein disulfide bond.

Steady-State Kinetic Analysis and pH−Rate Behavior. Initial velocity data from assays in which the concentration of one substrate was varied at various fixed levels of the cosubstrate showed a pattern of parallel lines in double-reciprocal plots (Figure 3). These data are most consistent with a ping-pong mechanism (see below). The steady-state

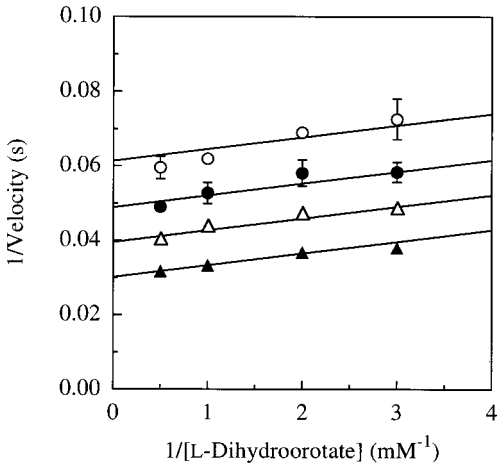

FIGURE 3: Initial velocity pattern for the NAD^+-dependent oxidation of L-DHO to orotate by *C. oroticum* DHO dehydrogenase. Initial velocities [M^{-1} (tetramer) s^{-1}] were determined in triplicate. The average reciprocal velocities and associated standard deviations are plotted as a function of the reciprocal concentrations of L-DHO. The solid lines are the best fits to an equation describing a ping-pong mechanism. The concentrations of NAD^+ used were 0.17 mM (○), 0.25 mM (●), 0.40 mM (△), and 1.0 mM (▲).

Table 1: Steady-State Kinetic Constants of *C. oroticum* Dihydroorotate Dehydrogenase[a]

k_{cat}[d]	$45 \pm 2\ s^{-1}$
K_m (L-DHO)[b]	$90 \pm 10\ \mu M$
K_m (NAD^+)[c]	$130 \pm 10\ \mu M$
k_{cat}/K_m (L-DHO)[b]	$(5.1 \pm 0.5) \times 10^5\ M^{-1}\ s^{-1}$
k_{cat}/K_m (NAD^+)[c]	$(3.5 \pm 0.3) \times 10^5\ M^{-1}\ s^{-1}$

[a] pH = 8.0, 25 °C (see Experimental Procedures). [b] At saturating NAD^+ concentration. [c] At saturating L-DHO concentration. [d] At saturating NAD^+ and L-DHO concentrations. The maximum turnover number, k_{cat}, is calculated on the basis of the concentration of enzyme tetramers.

kinetic constants reported in Table 1 were obtained from replots of the slopes and *Y*-intercepts of these data (Figure 3) assuming a ping-pong mechanism. The steady-state kinetic constants obtained at pH = 8.0 (Table 1) compare favorably with those measured previously at pH = 6.8 (*23*). The maximum turnover number of 45 s^{-1} is similar to 29 s^{-1}, and the K_m values for L-DHO and NAD^+ (of 90 and 130 μM, respectively) are similar to those reported before (170 and 360 μM, respectively). The small differences are probably due to the different pH values at which the experiments were done (see Figure 4).

The pH dependence of k_{cat} is shown in Figure 4A, while that of $k_{cat}/K_{m(DHO)}$ is shown in Figure 4B. The observed pH−rate behavior reflected ionizations of the enzyme since L-DHO has no ionizable groups in this pH range [the pK_a of the carboxylic acid group of L-DHO is 3.0, while that of the N−H groups is ≥11.5 (*24*)]. Moreover, appropriate controls showed that the concentrations of activating L-cysteine and substrate NAD^+ were essentially saturating over the pH range examined (Experimental Procedures). The value of k_{cat} decreases below a single pK_a of 6.4 ± 0.1 and above a single pK_a of 8.9 ± 0.1 when the data are fitted to eq 3 (Experimental Procedures). $k_{cat}/K_{m(DHO)}$ also decreases at low and high pH, but in this case eq 3 gives a poor fit to the data (dashed line) with pK_as of 6.5 ± 0.1 and 8.9 ± 0.2. Equation 4 (Experimental Procedures) gives a better fit (solid line) with the following four pH-dependent terms: pK_A = 6.1 ± 0.3, pK_B = 7.3 ± 0.2, pK_C = 5.1 ± 0.4, and pK_D = 8.6 ± 0.1.

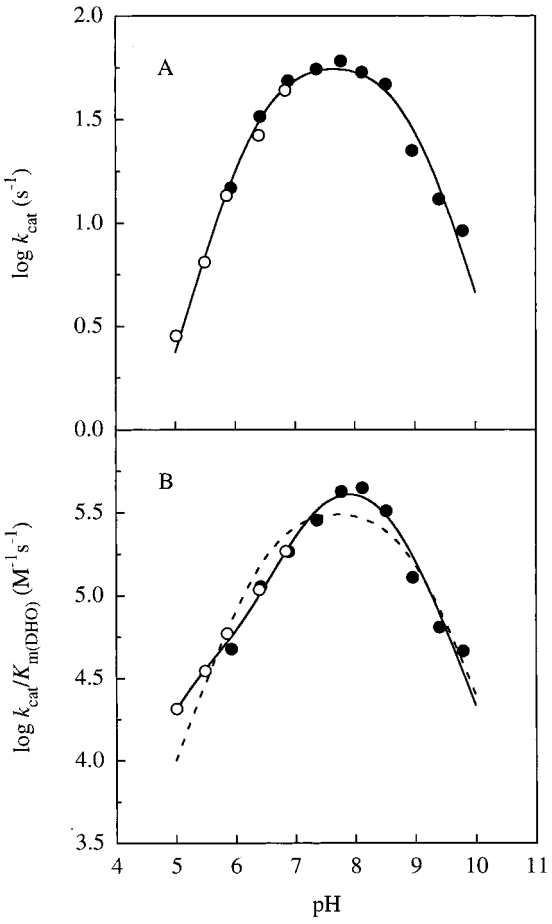

FIGURE 4: Dependence of k_{cat} and $k_{cat}/K_{m(DHO)}$ on pH. (A) pH variation of k_{cat} fitted to eq 3; pK_B = 6.4 ± 0.1, pK_D = 8.9 ± 0.1, and $C = 61 \pm 4\ s^{-1}$. (B) pH variation of $k_{cat}/K_{m(DHO)}$ with L-DHO as the variable substrate and NAD^+ kept at a saturating level (2 mM). Data were fitted to eq 3 [dotted line; pK_B = 6.5 ± 0.1, pK_D = 8.9 ± 0.2, $C = (3.5 \pm 0.7) \times 10^5\ M^{-1}\ s^{-1}$] and eq 4 [solid line; pK_A = 6.1 ± 0.3, pK_B = 7.3 ± 0.2, pK_C = 5.1 ± 0.4, pK_D = 8.6 ± 0.1, $C = (5.8 \pm 1.1) \times 10^5\ M^{-1}\ s^{-1}$]. The buffers used were 50 mM phosphate/50 mM acetate (○) and 50 mM phosphate/50 mM bis-tris propane (●) with sufficient pH overlap. The pH was measured after the reactions were complete.

Kinetic Isotope Effects. The pH dependence of the deuterium kinetic isotope effect arising from deuterium substitution at C_5 of L-DHO (**7** in Figure 1) at saturating concentrations (2 mM) of NAD^+ is shown in Figure 5. Both ^DV and $^D(V/K_{DHO})$ increase from a value of unity at high pH to sizable values at low pH. Limiting values at low pH were 1.34 ± 0.02 (for ^DV) and 1.9 ± 0.1 [for $^D(V/K_{DHO})$]. The pH at which the isotope effect is half the value at low pH is 7.7 ± 0.2 (for ^DV) and 7.2 ± 0.3 [for $^D(V/K_{DHO})$].

To address whether the mechanism was stepwise or concerted (see Discussion), we also determined the isotope effects for substrates **4**−**6**. These studies were conducted at pH = 6.5, where the isotope effects for **7** were sizable. Double-reciprocal plots with L-DHO as the variable substrate for substrates **1** and **5**−**7** are shown in Figure 6A, and the results are summarized in Table 2. The effect of deuterium substitution at the C_5-*proR* position when C_5-*proS*−H and C_6−H are both deuterated is shown in Figure 6B (triangles). As expected, the secondary deuterium kinetic isotope effects on *V* (1.17 ± 0.13) and V/K_{DHO} (1.00 ± 0.13) are very small.

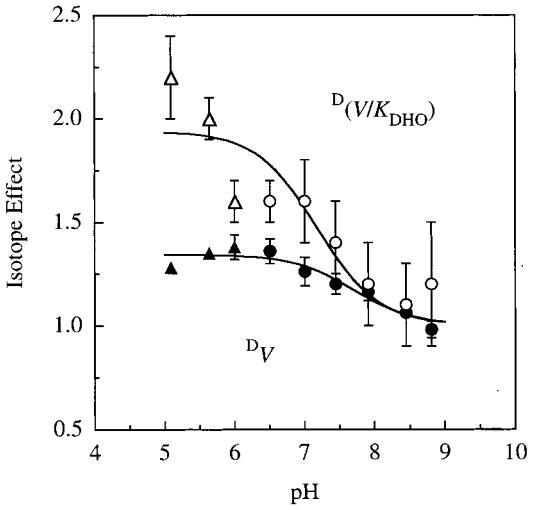

FIGURE 5: pH variation of the steady-state deuterium kinetic isotope effect on V_{max} (^{D}V) and $V_{max}/K_{m(DHO)}$ [$^{D}(V/K_{DHO})$] for L-[5*R*,5*S*-$^{2}H_2$]-DHO (**7**). Data were fitted to eq 5 with $IE_{LpH} = 1.9 \pm 0.1$, $pK_a = 7.2 \pm 0.3$ [for $^{D}(V/K)$] and $IE_{LpH} = 1.34 \pm 0.02$, $pK_a = 7.7 \pm 0.2$ [for ^{D}V]. Buffers used were 50 mM phosphate/50 mM acetate (△, ▲) and 50 mM phosphate/50 mM bis-tris propane (○, ●).

Several potential sources of error must be considered when isotope effects are performed by direct comparison of the initial velocities of turnover of a protonated versus a deuterated substrate, including substrate purity, isotopic enrichment, and substrate concentration (*25*). All of the selectively deuterium-labeled substrates synthesized in the present study were crystallized and had melting points which were indistinguishable from literature values. Moreoever, we confirmed that **1** from commercial sources gave velocities identical to those of **1** synthesized enzymatically from orotate, followed by purification and crystallization according to the same procedures used for substrates **4**−**7** (Figure 6B, filled versus open circles). Solutions of each substrate in Me_2SO-d_6 showed only the expected substrate ^{1}H NMR peaks (and those of the NMR solvent; data not shown), and deuterium enrichment was >96% at all relevant substrate positions (Experimental Procedures). The concentrations of substrates were determined by enzymatic end-point assays to within ≤±3% of the average value. Thus, the observed rate differences (Figures 5 and 6A, Table 2) are due to the nature of the isotopic substitution rather than to the coisolation of an inhibitor or activator, variations in substrate concentration, or variable isotopic enrichment.

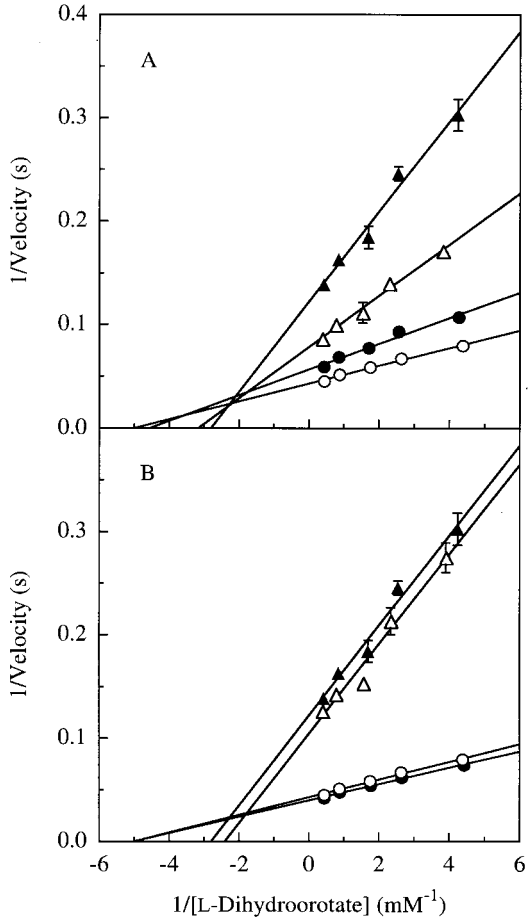

FIGURE 6: Double-reciprocal plots for the NAD^+-dependent DHO dehydrogenase activity with various deuterium-labeled L-DHO substrates. Panel A illustrates the presence of significant deuterium kinetic isotope effects on both ^{D}V and $^{D}(V/K_{DHO})$. Data are for **1** (○), **7** (●), **5** (△), and **6** (▲). Panel B illustrates (a) that the initial rates for enzymatically synthesized L-DHO (**1**) and **1** from commercial sources are indistinguishable and (b) that the secondary deuterium kinetic isotope effect arising from the C_5-*proR* position is very small. Data are for enzymatically synthesized **1** (○), **1** from commercial sources (●), **4** (△), and **6** (▲). The solid lines are linear least-squares fits of the data to eq 2. All points are the average of three determinations with the standard deviations shown by the error bars. Assays were conducted at saturating (2 mM) NAD^+ concentration at pH = 6.5 and 25 °C using the 50 mM phosphate/50 mM bis-tris propane buffer system as described under Experimental Procedures.

DISCUSSION

Characterization of the C. oroticum DHO Dehydrogenase. We chose the *C. oroticum* DHO dehydrogenase for our mechanistic studies primarily on the basis of its expected ease of purification. An additional advantage of the *C. oroticum* enzyme was that, as anticipated from its ability to use NAD^+ as a terminal electron acceptor, it proved to belong to the heterotetrameric (1B) family of DHO dehydrogenases. Multiple substrate kinetic isotope effects have not previously been reported for any member of this enzyme subfamily (see below).

The 32 and 28 kDa polypeptides associated with the purified enzyme represent the α and *β* subunits, respectively, of a high-affinity heterooligomer. This conclusion follows from the resistance of the two polypeptides to separation by chromatography on several types of columns, plus their precise coelution with NADH-dependent orotate reductase activity and yellow color. The apparent native molecular mass of ≈120 kDa by size exclusion chromatography (see Results) and equilibrium sedimentation and the apparent 1:1 ratio of the two polypeptides suggest that the native enzyme is a heterotetramer consisting of two α and two *β* subunits. These conclusions are strengthened by the striking similarity between the *C. oroticum* DHO dehydrogenase and the family 1B DHO dehydrogenases from *L. lactis*, *E. faecalis*, and *B. subtilis*.

The genes encoding the two polypeptides (PyrDB [α] and PyrK [*β*]) of the *L. lactis* (*7*) and *B. subtilis* (*8*) DHO dehydrogenase B enzymes have been cloned and sequenced, and the proteins have been purified following expression in *E. coli*. When expressed alone, PyrDB was an unstable

Table 2: Steady-State Kinetic Isotope Effects for *C. oroticum*, *C. fasciculata*, and Bovine Liver Mitochondrial Dihydroorotate Dehydrogenases

		C. oroticum[a]		*C. fasciculata*[b]		bovine[c]	
no.	substrates compared	$^{D}(V/K_{DHO})$	^{D}V	$^{D}(V/K_{DHO})$	^{D}V	$^{D}(V/K_{DHO})$	^{D}V
1	$^{5}H_RH_S$-^{6}H vs $^{5}D_RD_S$-^{6}H	1.51 ± 0.07	1.34 ± 0.02	3.25 ± 0.06	2.83 ± 0.06	2.95 ± 0.42	2.92 ± 0.16
2	$^{5}H_RH_S$-^{6}H vs $^{5}H_RH_S$-^{6}D	2.94 ± 0.07	1.92 ± 0.09	2.99 ± 0.08	2.98 ± 0.07	1.31 ± 0.12	1.71 ± 0.06
3a	$^{5}H_RH_S$-^{6}H vs $^{5}D_RD_S$-^{6}D	5.44 ± 0.37	2.96 ± 0.12	6.79 ± 0.15	8.03 ± 0.10	3.90 ± 0.60	4.50 ± 0.30
3b	1 × 2	4.44 ± 0.23	2.57 ± 0.13	9.72 ± 0.31	8.44 ± 0.28	3.86 ± 0.70	4.99 ± 0.30
4a	$^{5}H_RH_S$-^{6}D vs $^{5}D_RD_S$-^{6}D	1.85 ± 0.09	1.55 ± 0.02	2.27 ± 0.07	2.67 ± 0.06	2.80 ± 0.36	2.45 ± 0.11
4b	$^{5}H_RH_S$-^{6}H vs $^{5}D_RD_S$-^{6}H	1.51 ± 0.07	1.34 ± 0.02	3.25 ± 0.06	2.83 ± 0.06	2.95 ± 0.42	2.92 ± 0.16
5a	$^{5}D_RD_S$-^{6}H vs $^{5}D_RD_S$-^{6}D	3.59 ± 0.08	2.22 ± 0.06	2.09 ± 0.05	2.83 ± 0.06	1.13 ± 0.14	1.32 ± 0.06
5b	$^{5}H_RH_S$-^{6}H vs $^{5}H_RH_S$-^{6}D	2.94 ± 0.07	1.92 ± 0.09	2.99 ± 0.08	2.98 ± 0.07	1.31 ± 0.12	1.71 ± 0.06

[a] This work. At 25 °C, pH = 6.5, and saturating levels (2 mM) of NAD^+ (see Experimental Procedures). Isotope effects are expressed as the ratios of V or V/K_{DHO} (and associated standard deviations) for the substrates compared, and the errors have been propagated as described by Skoog and West for indeterminate errors (*44*). [b] Data from Pascal et al. (*2*). [c] Data from Hines et al. (*13*).

homodimeric enzyme containing one molecule of FMN per subunit; it could transfer electrons from L-DHO to ferricyanide but not to NAD^+. Coexpression of the PyrDB and PyrK subunits gave a stable $\alpha_2\beta_2$ heterotetramer that utilized NAD^+ as an electron acceptor. These enzymes and the *E. faecalis* (*9*) enzyme use the same cofactors as the *C. oroticum* DHO dehydrogenase, namely, two molecules of FMN, two molecules of FAD, four iron atoms, and four "labile" sulfur atoms per tetramer.

Insight into the molecular roles of these cofactors is provided by the crystal structure (*26*) of the heterotetrameric B enzyme from *L. lactis* with bound product orotate, which is shown schematically in Figure 7A (K. F. Jensen, personal communcation).[2] The FMN is located on the PyrDB subunit while FAD resides on the PyrK subunit. The iron−sulfur cluster also resides on the PyrK subunit; it is close to the heterosubunit interface, roughly midway between the two flavins which are about 19 Å apart. Orotate binds at the FMN site. Based on these structural data, it is reasonable to propose that there are two active sites per tetramer, with each active site harboring one molecule of FMN, one molecule of FAD, and one iron−sulfur [Fe_2S_2] cluster. L-DHO would be oxidized to orotate by transferring a pair of electrons to FMN. It is likely that the electrons are then transferred to NAD^+ at the FAD site via the iron−sulfur cluster (Figure 7B), although there is as yet no direct evidence to support NAD^+ binding at the FAD site. A similar architecture and mechanism is expected for the *C. oroticum* DHO dehydrogenase.

Steady-State Kinetic Mechanism. The pattern of nearly parallel lines obtained in the steady-state kinetic analysis of DHO dehydrogenase (Figure 3) is consistent with a ping-pong mechanism (Scheme 2). A distinguishing feature of this mechanism is the absence of the ternary complexes L-DHO·E_{OX}·NAD^+ and OA·E_{RED}·NADH. While certain sequential mechanisms ($K_{ia} \ll K_{m_A}$, where K_{ia} is defined in Scheme 2 and K_{m_A} is the concentration of A giving half-maximal activity) can give reciprocal initial velocity plots that appear parallel, we do not favor these mechanisms for reasons discussed below.

Isotope effects on V/K are also useful to distinguish between different steady-state kinetic mechanisms. With L-DHO selectively deuterated at both the C_5-*proR* and C_5-*proS* positions (**7**), $^{D}(V/K_{DHO}) = 1.51 \pm 0.07$ while $^{D}(V/K_{NAD^+}) = 1.11 \pm 0.07$ (data not shown). An isotope effect of unity on one substrate's V/K (here, NAD^+) eliminates

Scheme 2

$$E_{OX} \underset{K_{ia}}{\overset{\pm \text{L-DHO}}{\rightleftharpoons}} E_{OX}\cdot\text{L-DHO} \rightleftharpoons E_{RED}\cdot\text{OA} \overset{\pm \text{OA}}{\rightleftharpoons} E_{RED}$$

$$E_{RED} \overset{\pm NAD^+}{\rightleftharpoons} E_{RED}\cdot NAD^+ \rightleftharpoons E_{OX}\cdot\text{NADH} \overset{\pm \text{NADH}}{\rightleftharpoons} E_{OX}$$

random and rapid equilibrium ordered mechanisms (*27*). In contrast, these data are consistent with a ping-pong mechanism, although they do not rule out a steady-state ordered mechanism with NAD^+, the substrate with $^{D}(V/K) = 1$, binding first.

Sequential mechanisms require the formation of a ternary complex (e.g., DHO·E_{OX}·NAD^+) before the chemical step, while ping-pong mechanisms do not (above). Thus, if the mechanism is ping-pong, DHO dehydrogenase should catalyze the interconversion of L-DHO and orotate in the absence of NAD^+ or NADH. Anaerobic incubation of DHO dehydrogenase at pH = 8.0 and 10 mM L-cysteine in the presence of 4 mM L-DHO and 1 mM [^{14}C]orotate (a saturating concentration of each), but without NAD^+ or NADH, resulted in the formation of L-[^{14}C]-DHO at a rate that was 18% of k_{cat} for the reverse reaction ($k_{catr} = 22\ s^{-1}$). This experiment provides strong evidence that the steady-state kinetic mechanism is ping-pong. That exchange occurred at a rate slower than k_{cat} may be explained by enzyme inhibition due to the high concentrations of substrate and product.

Finally, ping-pong mechanisms have been proposed for all DHO dehydrogenases studied thus far. These include the DHO dehydrogenase B from *E. faecalis* (*9*) and the family 2 *E. coli* (*28*) and bovine liver mitochondrial (*29*) DHO dehydrogenases. A nonclassical two-site ping-pong mechanism has also been proposed for the dihydropyrimidine dehydrogenase from pig liver (*30*) which catalyzes the $NADP^+$-dependent oxidation of dihydrouracil and dihydrothymine to uracil and thymine, respectively. This enzyme resembles the family 1B DHO dehydrogenases in that it also features FMN, FAD, and iron atoms that are probably present as iron−sulfur clusters.

Interpretation of the pH Profiles. The pH profiles presented in Figure 4 show that there is a single group with a pK_a of about 7 which must be deprotonated for activity. There is another group with a pK_a of about 8.9 that must be protonated for activity. The apparent pK_as of these groups are observed in both k_{cat} and $k_{cat}/K_{m(DHO)}$ profiles. These groups must reside on the enzyme because the substrate L-DHO does not have an ionizable group in this pH range (see Results).

[2] Based on information generously provided by K. F. Jensen.

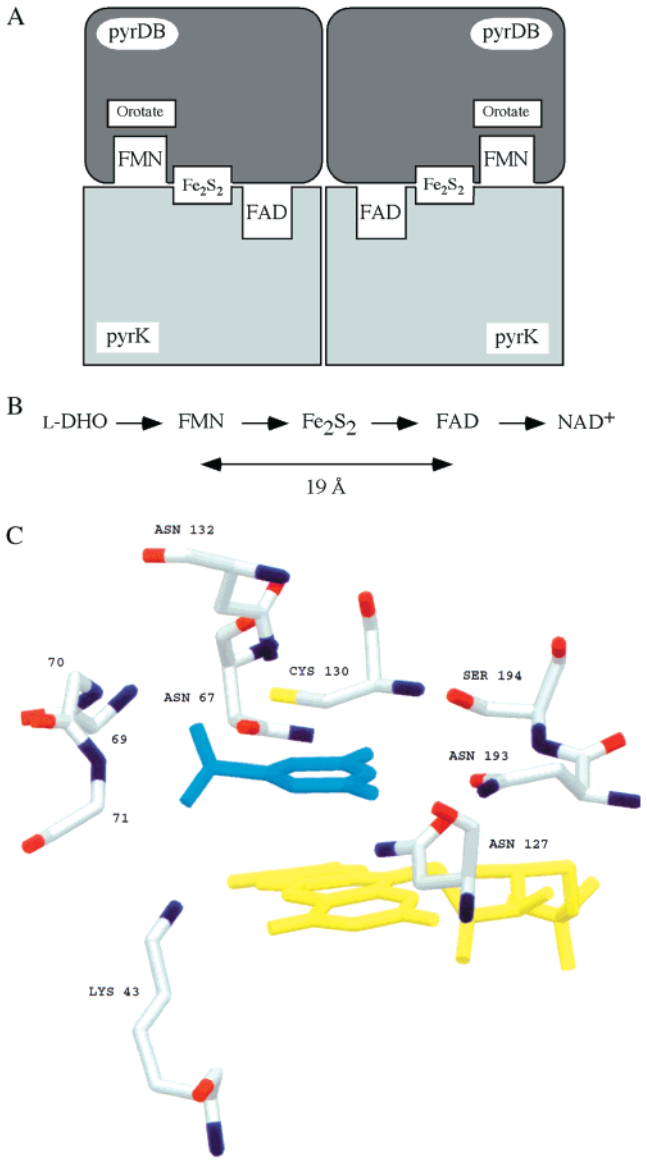

FIGURE 7: (A) Quaternary structure of the *L. lactis* DHO dehydrogenase B enzyme. The cartoon is based on the crystal structure of this enzyme complexed with the product orotate.[2] The FMN resides on the PyrDB subunit while FAD is on the PyrK subunit. The iron−sulfur cluster also resides on the PyrK subunit and is close to the heterosubunit interface, midway between the two flavins which are about 19 Å apart. Orotate binds at the FMN site. (B) Proposed pathway for electron transfer. L-DHO is oxidized to orotate by transferring a pair of electrons to FMN. The electrons are then transferred to the ultimate electron acceptor, NAD^+, at the FAD site via the iron−sulfur cluster. (C) Active site of DHO dehydrogenase A from *L. lactis* based on the crystal structure of this enzyme with bound orotate. The product orotate is stacked above the flavin isoalloxazine ring system. Orotate makes hydrogen bonds with the four conserved asparagine side chains (Asn-67, Asn-127, Asn-132, and Asn-193), the side chains of Lys-43 and Ser-194, and the main chain NH groups of Met-69, Gly-70, and Leu-71. Cys-130 is 3.3 Å away from C_5 of orotate and in perfect position to be the general base that abstracts the C_5-*proS* proton of L-DHO and thus initiates the *trans*-dehydrogenation of the substrate. Lys-43 is 2.8 Å away from one of the C_6-carboxylate oxygens of L-DHO.

Below pH 7, the $k_{cat}/K_{m(DHO)}$ curve is flattened, and eq 3 fits the data poorly (Figure 4, panel B, dotted line). Equation 4, on the other hand, fits the data much better. The fitted (solid) line shows what has been termed a "hollow" (*31*). The data are interpreted in the context of Scheme 3 as

Scheme 3

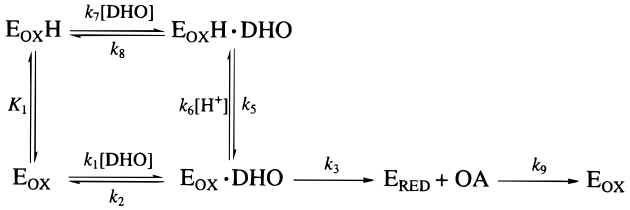

described by Cook et al. for creatine kinase (*32*). In Scheme 3, k_3 represents the only deuterium-sensitive step, but it is not a microscopic rate constant—it may contain isomerization steps. Likewise, k_9 represents product orotate release and regeneration of oxidized enzyme (E_{OX}) by NAD^+ combined, for simplicity, into one step.

Cook et al. showed that a hollow will be observed in the V/K pH profile if both the substrate and the proton in the E−H·S complex ($E_{OX}H \cdot DHO$ in the present case) are sticky. They further showed that pK_A and pK_C of eq 4 can be used to estimate the stickiness (k_3/k_2) of the substrate, $k_3/k_2 = 10^{pK_A - pK_C} - 1$. From the fits to eq 4, $pK_A = 6.1$ and $pK_C = 5.1$, yielding $k_3/k_2 = 9$. The ratio $k_3/k_2 = 9$ suggests that the substrate L-DHO is sticky; that is, it forms products about nine times faster than it dissociates from the $E_{OX} \cdot DHO$ complex. The isotope effect observed for a sticky substrate should be pH dependent (*33*, *34*), as observed in the present case (below).

Isotope Effects. The high commitment (*35*) to catalysis ($k_3/k_2 = 9$) will depress any observed isotope effect [$^DV/K = (^Dk_3 + k_3/k_2)/(1 + k_3/k_2)$] from the intrinsic value, $^Dk_3$. Theory has previously been developed for the dependence of isotope effects on pH (*33*, *34*), and for the mechanism in Scheme 3, both ^DV and $^DV/K$ should be equal to the intrinsic value [$^Dk_3$] at low pH. At high pH the observed isotope effects will be depressed from the intrinsic value according to the following expressions (*33*, *34*): $^DV = (^Dk_3 + k_3/k_9)/(1 + k_3/k_9)$ and $^DV/K = (^Dk_3 + k_3/k_2)/(1 + k_3/k_2)$. The isotope effects on V and V/K_{DHO} for **7** are unity at high pH and increase to a pH-independent value at low pH as predicted by theory and confirming that the substrate, L-DHO, is sticky. However, as can be seen from Figure 5, the isotope effects on V and V/K_{DHO} at low pH are not equal and are not likely to be intrinsic values. This apparent contradiction can be reconciled if another step is partly rate limiting over the entire pH range but becomes more rate limiting at high pH. This step might be product orotate release or regeneration of oxidized enzyme by NAD^+. A similar situation has been observed for L-alanine dehydrogenase from *B. subtilis* where both V/K_{Ala} and V increase at low pH; the isotope-insensitive step which is more rate limiting at high pH was proposed to be either product release or isomerization of the $E \cdot NAD^+$ complex (*36*).

The crystal structure of the *L. lactis* DHO dehydrogenase A enzyme (family 1A) has been solved with (*37*) and without (*4*) bound product orotate. In the active site (Figure 7C), there are only two residues with acid/base properties typical of general acids and bases. One of these, Cys-130, is 3.3 Å from C_5 of orotate, while the other, Lys-43, is 2.8 Å from one of the carboxylate oxygens of orotate. Cys-130 and Lys-43 are both completely conserved in family 1 enzymes (*4*). The activity of the C130S mutant of the A enzyme is reduced by a factor of 10^4 at pH = 8.0 but only 10^2 at pH = 10 (*21*).

It was proposed that Cys-130 was the general base that abstracts the C_5-*proS* proton and that Ser-130, in the mutant, substitutes for cysteine at high pH. The K43E and K43A mutant enzymes have 10^3-10^4 lower $k_{cat}/K_{m(DHO)}$ values than wild type (*21*). These findings suggest that Cys-130 and Lys-43 both play critical roles in catalysis.

The anticipated active site structure of the *C. oroticum* DHO dehydrogenase (Figure 7) provides an attractive explanation of the pH−rate data shown in Figures 4 and 5. The pK_a of 6.4−7.7 in the pH−rate and pH−isotope effect profiles may be assigned to a cysteine residue that must be deprotonated in order to abstract the C_5-*proS* proton of L-DHO. Likewise, the pK_a of 8.9 may be assigned to a lysine residue and has to be protonated (positively charged) for activity. The role(s) of the lysine may include both substrate binding (favorable electrostatic interaction with the C_6-carboxylate group of L-DHO) and transition-state stabilization, since both k_{cat} and k_{cat}/K_m decrease at high pH. Confirmation of the presence of these residues in the active site, and validation of their proposed catalytic roles, will require the cloning and sequencing of the genes encoding the α and β subunits of the *C. oroticum* enzyme.

Multiple Isotope Effects. The concerted or stepwise nature of enzyme-catalyzed reactions can be probed using multiple isotope effects (*38*−*40*). Deuterium substitution at position 1 will have a different effect on the isotope effect observed on position 2, depending on whether the mechanism is stepwise or concerted. In a stepwise mechanism, slowing down step 1 (proton transfer in Scheme 1) relative to step 2 (hydride transfer) by deuterium substitution will decrease the observed isotope effect on step 2 (and vice versa). On the other hand, in a concerted mechanism deuterium substitution at position 1 will either (i) enhance the observed isotope effect on position 2 (because the chemical step has become slower or more rate limiting) or (ii) show no change if the chemical step was originally largely rate limiting.

We have used this approach to probe the stepwise or concerted nature of the *C. oroticum* DHO dehydrogenase mechanism. Isotope effects on substrates **4**−**7** were measured at pH = 6.5 (Table 2) where sizable isotope effects were observed for **7**. Deuterium substitution at C_5, C_6, or both led to significant isotope effects on both ^DV and $^D(V/K_{DHO})$ (Table 2, rows **1**−**3a**). The isotope effect at C_5 increased from 1.51 to 1.85 for $^D(V/K_{DHO})$ when C_6−H was substituted by C_6−D (row **4a** versus **4b**). Likewise, the isotope effect at C_6 increased from 2.94 to 3.59 when C_5−H was substituted by C_5−D (row **5a** versus **5b**). These results are consistent with a concerted mechanism of catalysis.

The same conclusion follows from a comparison of observed multiple isotope effects with the product of the individual isotope effects. For a stepwise mechanism, the product of the individual isotope effects should be larger than the effect observed upon multiple substitution. For a concerted mechanism, the product is either (i) smaller than the observed (if an isotope-insensitive step is partly rate limiting) or (ii) equal to the observed (if the isotope-sensitive step was originally largely rate limiting). Comparison of rows **3a** with **3b** in Table 2 shows that the product of the individual isotope effects is smaller than the observed multiple isotope effect.

Taken together, these results do not support a stepwise chemical mechanism and conform to the multiple isotope effects predicted for a concerted mechanism in which the chemical step is not fully rate limiting, as described above. The partially rate-limiting, isotope-insensitive step must come after the chemical step because ^DV is less than $^D(V/K_{DHO})$ even with the multiply deuterated sustrate (Table 2, row **3a**). These results are consistent with those from Figure 5 where ^DV is less than $^D(V/K_{DHO})$ for **7** from pH = 5.0−9.0. This step may be release of product orotate or regeneration of the oxidized enzyme by NAD^+.

Anaerobic, enzyme-catalyzed C_5-*proS*−L and C_6−L (L = H or D) hydron exchange with solvent in the absence of the ultimate electron acceptors has been carried out previously with the *C. oroticum* (*1*) and *C. fasciculata* (*2*) enzymes. ^{1}H NMR showed that, with both enzymes, exchange at C_5 occurred twice as fast as exchange at C_6. These experiments were interpreted to suggest the stepwise abstraction of the C_5-*proS*−H proton to generate the C_5-carbanion/enolate intermediate, which is either (1) reprotonated by a solvent hydron or (2) oxidized to form orotate at about half the rate as reprotonation. However, these experiments can also be consistent with a concerted mechanism if there are differential rates of exchange of the abstracted C_5−H and C_6−H protons from their respective sites in the E_{RED}·orotate complex. This situation could arise if, when orotate is bound, the general base which abstracts the C_5-*proS* proton is more solvent accessible than N_5 of the flavin which accepts the hydride. We favor this explanation for the *C. oroticum* enzyme since the isotope effects dictate a concerted mechanism.

As discussed in the introduction, the C_5-carbanion/enolate arising from C_5-*proS*−H proton abstraction is not stable enough to exist as a kinetically competent intermediate unless it is stabilized on the enzyme by at least 1.7 pK units. In our nonenzymatic model studies, we showed that the Brønsted coefficient (β) for deprotonating the C_5-*proS* proton was ≈0.8 (*12*). The relatively large value of β indicates that substantial rate enhancement ($10^{0.8\Delta pK_a}$ versus a maximum of $10^{\Delta pK_a}$) of proton abstraction can be achieved for a given increase in thermodynamic driving force (*41*). However, although the rate of acceleration that could be harnessed by stabilizing the intermediate C_5-carbanion/enolate is substantial, the *C. oroticum* DHO dehydrogenase evolved to utilize a concerted mechanism. This mechanism can be rationalized on the basis of the anticipated organization of the active site, as inferred from the crystal structure of the *L. lactis* DHO dehydrogenase A enzyme (Figure 7C). The C_4-carbonyl oxygen of orotate is hydrogen-bonded to the weakly acidic side chains of Asn-127 and Asn-193. As a result, there should be little polarization of the C_4-carbonyl oxygen of L-DHO, and limited stabilization of the C_5-enolate intermediate will be possible. The side chain amino group of Lys-43 is not close enough (6.3 Å) to play this role. In contrast, the positioning of Cys-130 and N_5 of FMN at opposite sides of the orotate ring is ideal to promote the concerted *trans*-dehydrogenation of L-DHO.

DHO Dehydrogenases: Correlation between Structure and Mechanism? Multiple isotope effects have previously been measured for the *C. fasciculata* (*2*) and bovine liver mitochondrial (*13*) DHO dehydrogenases (Table 2). There are notable differences among the results obtained with the three enzymes. Whereas our data for the *C. oroticum* enzyme support a concerted mechanism (above), the data for the *C.*

fasciculata enzyme favor a stepwise mechanism. Although the errors in the measurements for the bovine enzyme are rather large, the ^{D}V isotope effects argue in favor of a stepwise mechanism. However, as pointed out by Pascal et al. (*2*), this analysis of multiple isotope effects relies heavily on the validity of the "rule of the geometric mean" (*42*) in which the magnitude of isotope effects at multiple positions in a reacting molecule is independent of one another. This rule may not hold for concerted mechanisms when coupled motion and hydrogen tunneling are involved. If proton transfer and hydride transfer occur in the same step and both hydrogen nuclei tunnel, then the first deuterium substitution will have a larger effect than subsequent deuterium substitutions, because it is the first substitution which drastically decreases the efficiency of hydrogen tunneling (*43*). Thus, the data for the *C. fasciculata* enzyme can also be explained by a concerted mechanism in which there is tunneling by the C_5-*proS*−H and C_6−H hydrogen nuclei. In contrast, we are not aware of any stepwise mechanism which can explain the data for the *C. oroticum* enzyme.

While the sequences of the *C. oroticum*, *C. fasciculata*, and bovine enzymes are not yet known, the *C. oroticum* enzyme is expected to be part of family 1B on the basis of its remarkable resemblance to the family 1B enzymes (above). The bovine enzyme can be placed in family 2 since it is mitochondrial; the *C. fasciculata* enzyme, though with less certainty, may be placed in family 1A on the basis of strong sequence similarity between the enzyme from a different parasite (*T. cruzi*) and the *L. lactis* A enzyme (*5*). Analysis of multiple isotope effects (above) suggests that the family 1B enzymes employ a concerted mechanism, whereas family 1A and 2 enzymes employ a stepwise mechanism. These results suggest that differences in mechanism, as well as in structure and electron acceptor, may distinguish DHO dehydrogenases belonging to families 1A, 1B, and 2. These mechanistic differences may ultimately prove useful in the design of species-specific inhibitors of DHO dehydrogenase.

ACKNOWLEDGMENT

We are grateful to Dr. Albert S. Mildvan for suggestions and help with the interpretation of some of the data and to Dr. John S. Blanchard for a critical reading of the manuscript. We thank Dr. Kaj Frank Jensen for communicating a description of the crystal structure of the *L. lactis* DHO dehydrogenase B enzyme prior to publication and Apostolos Gittis for preparing Figure 7C. We also thank the Microbiology Division of the Department of Pathology (The Johns Hopkins University) for use of the anaerobic incubator. NMR studies were performed in the Biochemistry NMR facility at The Johns Hopkins University, which was established by grants from the National Institutes of Health (GM 27512 and RR 06261).

REFERENCES

1. Blattmann, P., and Retey, J. (1972) *Eur. J. Biochem. 30*, 130−137.
2. Pascal, R. A., Jr., and Walsh, C. T. (1984) *Biochemistry 23*, 2745−2752.
3. Lieberman, I., and Kornberg, A. (1953) *Biochim. Biophys. Acta 12*, 223−234.
4. Rowland, P., Nielsen, F. S., Jensen, K. F., and Larsen, S. (1997) *Structure 5*, 239−252.
5. Gao, G., Nara, T., Nakajima-Shimada, J., and Aoki, T. (1999) *J. Mol. Biol. 285*, 149−161.
6. Nielsen, F. S., Rowland, P., Larsen, S., and Jensen, K. F. (1996) *Protein Sci. 5*, 852−856.
7. Nielsen, F. S., Andersen, P. S., and Jensen, K. F. (1996) *J. Biol. Chem. 271*, 29359−29365.
8. Kahler, A. E., Nielsen, F. S., and Switzer, R. L. (1999) *Arch. Biochem. Biophys. 371*, 191−201.
9. Marcinkeviciene, J., Tinney, L. M., Wang, K. H., Rogers, M. J., and Copeland, R. A. (1999) *Biochemistry 38*, 13129−13137.
10. Thibblin, A., and Jencks, W. P. (1979) *J. Am. Chem. Soc. 101*, 4963−4973.
11. Jencks, W. P. (1980) *Acc. Chem. Res. 13*, 161−169.
12. Argyrou, A., and Washabaugh, M. W. (1999) *J. Am. Chem. Soc. 121*, 12054−12062.
13. Hines, V., and Johnston, M. (1989) *Biochemistry 28*, 1227−1234.
14. Miller, C. S., Gordon, T., and Engelhardt, E. L. (1953) *J. Am. Chem. Soc. 75*, 6086−6087.
15. Smith, P. K., Krohn, R. I., Hermanson, G. T., Mallia, A. K., Gartner, F. H., Provenzano, M. D., Fujimoto, E. K., Goeke, N. M., Olson, B. J., and Klenk, D. C. (1985) *Anal. Biochem. 150*, 76−85.
16. Friedmann, H. C., and Vennesland, B. (1960) *J. Biol. Chem. 235*, 1526−1532.
17. Kondo, H., Friedmann, H. C., and Vennesland, B. (1960) *J. Biol. Chem. 235*, 1533−1535.
18. Haldeman, M. T., Xia, G., Kasperek, E. M., and Pickart, C. M. (1997) *Biochemistry 36*, 10526−10537.
19. Krakow, G., and Vennesland, B. (1961) *J. Biol. Chem. 236*, 142−144.
20. Aleman, V., and Handler, P. (1967) *J. Biol. Chem. 242*, 4087−4096.
21. Bjornberg, O., Rowland, P., Larsen, S., and Jensen, K. F. (1997) *Biochemistry 36*, 16197−16205.
22. Claiborne, A., Miller, H., Parsonage, D., and Ross, R. P. (1993) *FASEB J. 7*, 1483−1490.
23. Miller, R. W., and Massey, V. (1965) *J. Biol. Chem. 240*, 1453−1465.
24. Sander, E. G. (1969) *J. Am. Chem. Soc. 91*, 3629−3634.
25. Parkin, D. W. (1991) in *Enzyme mechanism from isotope effects* (Cook, P. F., Ed.) pp 269−290, CRC Press, Boca Raton, FL.
26. Jensen, K. F., and Bjornberg, O. (1998) *Paths Pyrimidines 6*, 20−28.
27. Cook, P. F. (1991) in *Enzyme mechanism from isotope effects* (Cook, P. F., Ed.) pp 203−230, CRC Press, Boca Raton, FL.
28. Bjornberg, O., Gruner, A.-C., Roepstorff, P., and Jensen, K. F. (1999) *Biochemistry 38*, 2899−2908.
29. Hines, V., and Johnston, M. (1989) *Biochemistry 28*, 1222−1226.
30. Podschun, B., Cook, P. F., and Schnackerz, K. D. (1990) *J. Biol. Chem. 265*, 12966−12972.
31. Cleland, W. W. (1977) *Adv. Enzymol. 45*, 273−387.
32. Cook, P. F., Kenyon, G. L., and Cleland, W. W. (1981) *Biochemistry 20*, 1204−1210.
33. Cook, P. F., and Cleland, W. W. (1981) *Biochemistry 20*, 1797−1805.
34. Cook, P. F. (1991) in *Enzyme mechanism from isotope effects* (Cook, P. F., Ed.) pp 231−245, CRC Press, Boca Raton, FL.
35. Northrop, D. B. (1977) in *Isotope effects on enzyme catalyzed reactions* (Cleland, W. W., O'Leary, M. H., and Northrop, D. B., Eds.) pp 140−141, University Park Press, Baltimore, MD.
36. Grimshaw, C. E., Cook, P. F., and Cleland, W. W. (1981) *Biochemistry 20*, 5655−5661.
37. Rowland, P., Bjornberg, O., Nielsen, F. S., Jensen, K. F., and Larsen, S. (1998) *Protein Sci. 7*, 1269−1279.

38. Blanchard, J. S., and Cleland, W. W. (1980) *Biochemistry 19*, 3543−3550.
39. Hermes, J. D., Roeske, C. A., O'Leary, M. H., and Cleland, W. W. (1982) *Biochemistry 21*, 5106−5114.
40. Belasco, J. G., Albery, W. J., and Knowles, J. R. (1983) *J. Am. Chem. Soc. 105*, 2475−2477.
41. Richard, J. P. (1998) *Biochemistry 37*, 4305−4309.
42. Bigeleisen, J. (1955) *J. Chem. Phys. 23*, 2264−2267.
43. Hermes, J. D., and Cleland, W. W. (1984) *J. Am. Chem. Soc. 106*, 7263−7264.
44. Skoog, D. A., and West, D. M. (1982) in *Fundamentals of Analytical Chemistry*, pp 75−80, Saunders College Publishing, Philadelphia, PA.

BI001111D